Journal of Magnetic Resonance **140,** 451–459 (1999)
Article ID jmre.1999.1852, available online at http://www.idealibrary.com on IDEAL®

Signal Enhancement Using 45° Water Flipback for 3D ^{15}N-Edited ROESY and NOESY HMQC and HSQC

James M. Gruschus and James A. Ferretti

Laboratory of Biophysical Chemistry, NHLBI, National Institutes of Health, Bethesda, Maryland 20892-0380

Received January 8, 1999; revised June 23, 1999

A novel implementation of the water flipback technique employing a 45° flip-angle water-selective pulse is presented. The use of this water flipback technique is shown to significantly enhance signal in 3D ^{15}N-edited ROESY in a 20 kDa complex of the vnd/NK-2 homeodomain bound to DNA. The enhancement is seen relative to the same experiment using weak water presaturation during the recovery delay. This enhancement is observed for the signals from both labile and nonlabile protons. ROESY and NOESY pulse sequences with 45° water flipback are presented using both HMQC and HSQC for the ^{15}N dimension. The 45° flipback pulse is followed by a gradient, a water selective 180° pulse, and another gradient to remove quadrature images and crosspeak phase distortion near the water frequency. Radiation damping of the water magnetization during the t_1 and t_2 evolution periods is suppressed using gradients. Water resonance planes from NOESY–HMQC and NOESY–HSQC spectra show that the HMQC version of the pulse sequences can provide stronger signal for very fast exchanging protons. The HSQC versions of the ROESY and NOESY pulse sequences are designed for the quantitative determination of protein–water crossrelaxation rates, with no water-selective pulses during the mixing time and with phase cycling and other measures for reducing axial artifacts in the water signal.

Key Words: **PFG (pulsed field gradients); protein–water crossrelaxation rates; radiation damping suppression; high molecular weight; water suppression.**

INTRODUCTION

As the size of macromolecular systems studied by NMR has increased, the usage of ROESY experiments to measure internuclear distances has become less prevalent. Nevertheless, ROESY experiments can complement NOESY experiments in large systems to provide dynamical information on macromolecular internal motions (*1–6*), hydration water–macromolecule interactions (*7–10*) and to aid in the stereospecific assignment of resonances (*11*). The drawback of ROESY for larger systems is the substantial loss of signal intensity that occurs due to faster T_2 relaxation. Recently, the water flipback (*12*) and WATERGATE solvent suppression (*13*) techniques have been employed with ROESY experiments on smaller molecules resulting in an increase in signal intensity (*14*). This combination of techniques allows one to avoid water presaturation and thereby significantly enhance the intensity of resonances that strongly interact with water. These ROESY experiments on smaller molecules employ a lengthy delay during which radiation damping is exploited to achieve water flipback. NOE crossrelaxation can occur during the delay, making this approach suitable only for smaller molecules since their NOE crossrelaxation rates are small. Here, we present a new ^{15}N-edited 3D ROESY experiment that incorporates WATERGATE and includes a novel form of water flipback that utilizes a 45° flip-angle water-selective pulse. In this new experiment no lengthy delay is required, making this ROESY pulse sequence suitable for higher molecular weight systems. Both HSQC and HMQC forms of the experiments are presented and the relative strengths of each compared. The corresponding NOESY experiments are also provided. The NOESY experiments differ from our previously reported NOESY–HMQC experiment (*15*), not just in the inclusion of 45° flipback, but particularly in the design of the NOESY–HSQC pulse sequence, the design of which makes it particularly appropriate for measuring water–macromolecular interactions. The signal enhancement provided by the new ROESY experiment is demonstrated by comparison with the water presaturation ROESY experiment for the vnd/NK-2 homeodomain DNA complex (20 kDa, PDB accession code 1NK3, BioMagResBank accession code 4141).

METHODS AND RESULTS

Figure 1 shows the 3D ^{15}N-edited ROESY–HSQC and ROESY–HMQC pulse sequences. Figure 2 shows the corresponding sequences for the NOESY–HSQC and NOESY–HMQC. Water flipback is initiated by the first water-selective, 45° flip-angle pulse. However, because the selective pulse is applied with a 90° phase relative to the first high-power pulse and because the faster exchanging protons can undergo a significant amount of exchange during the selective pulse, small quadrature artifacts can appear in the signals of these faster exchanging protons. To remove these artifacts, and also phase distortions caused by the selective pulses on resonances near the water frequency, the 45° pulse is followed by a

1090-7807/99

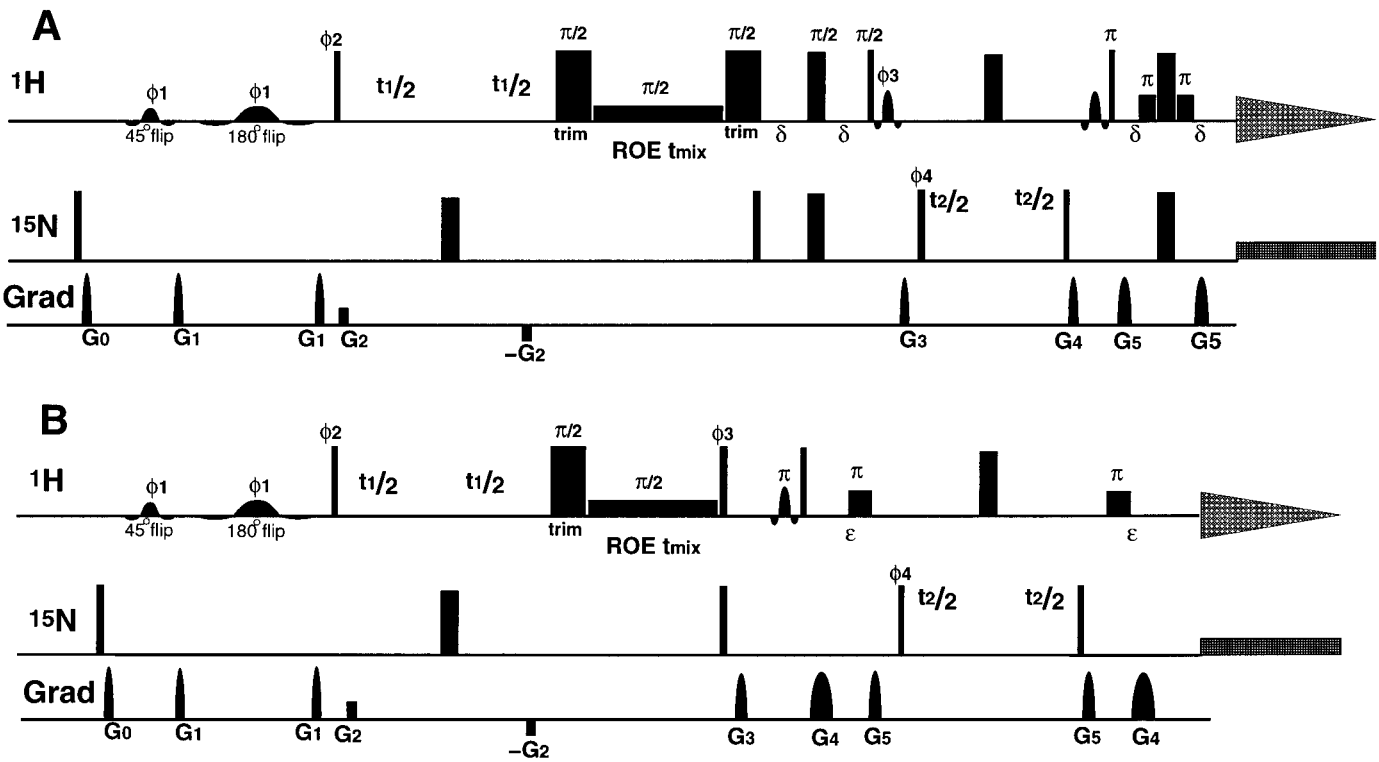

FIG. 1. Pulse sequences for the 3D ^{15}N-edited ROESY–HSQC and ROESY–HMQC with 45° water flipback. The tall, narrow rectangles correspond to high-power 90° ^{1}H and ^{15}N pulses, and the broader, tall rectangles correspond to high-power 180° ^{1}H and ^{15}N pulses, except for the pulses marked "trim." Each high-power ^{1}H trim (spin-lock purge) pulse is applied for 1 ms, contributing 1 ms each to the total mixing time. The mixing time low-power spin-lock pulse has a strength of 2.5 kHz. The short, broad rectangles correspond to low-power rectangular 90° pulses (~1 ms, 250 Hz). The taller ^{1}H shaped pulses, during the HSQC and before the HMQC portions of the pulse sequences, are sinc-shaped 90° pulses of ~2 ms duration. The longer ^{1}H shaped pulses at the beginning of the sequences are a sinc-shaped 45° flip-angle pulse of ~6–7 ms duration and a sinc-shaped 180° flip-angle pulse at the same power of ~20–22 ms duration. All pulses are applied at zero phase unless otherwise indicated. All ^{1}H pulses are applied at the carrier (H_2O) frequency. The rectangular gradient G2 has a strength of 2.5 G/cm along each axis and is in the $(+x, +y, +z)$ direction with a duration of 50 μs, followed by a delay of 50 μs. The initial t_1 time was set to a two-dwell delay in order to provide enough time for G2 and its delay. The sine bell shaped gradients are triple-axis, along $(+x, +y, +z)$, $(-x, +y, +z)$, $(+x, -y, +z)$, $(-x, -y, +z)$, and $(+x, +y, +z)$ for G0, G1, G3, G4, and G5, with strengths of 25 G/cm along each axis and each followed by a delay of 0.5 ms. The phases for the ROESY–HSQC (A) are $\phi_1 = \pi/4, \pi/4, 5\pi/4, 5\pi/4$; $\phi_2 = 7\pi/4, 7\pi/4, 3\pi/4, 3\pi/4$; $\phi_3 = \pi, \pi, 0, 0$; $\phi_4 = 0, \pi$; acq. $= \pi, 0, 0, \pi$. The States–TPPI protocol was used for phase-sensitive detection in the t_1 dimension by decrementing ϕ_1 and incrementing ϕ_2 by $\pi/2$ (also see Fig. 3). After each complex t_1 point, ϕ_3 is incremented by π. The TPPI protocol was used in the t_2 dimension by incrementing ϕ_4. The durations of G0, G1, G3, G4, and G5 are 0.3, 0.18, 0.25, 0.2, and 0.4 ms, and each gradient is followed by a 0.5 ms delay. The delay $\delta = 2.2$ ms. For the ROESY–HMQC (B) the phases are $\phi_1 = \pi/4, \pi/4, 5\pi/4, 5\pi/4$; $\phi_2 = 7\pi/4, 7\pi/4, 3\pi/4, 3\pi/4$; $\phi_3 = 0, 0, \pi, \pi$; $\phi_4 = 0, \pi$; acq. $= 0, \pi$. Phase sensitive detection in t_1 and t_2 is done as in (A), except that both ϕ_3 and the acquisition phase are incremented by π after each complex t_1 point. The durations of G0, G1, and G2 are the same as (A), and for G3, G4, and G5 the durations are 0.25, 3.0, and 0.2 ms. The directions of the gradients and the delays following them are the same as in (A). The delay $\epsilon = 4.5$ ms.

gradient, a water-selective 180° pulse, and another gradient. Both of these gradients (G1 in Fig. 1) are of the same length and direction. This gradient, selective 180° pulse, gradient sequence suppresses the quadrature images and phase distortions by dephasing all nonlongitudinal magnetization before the first 90° pulse of the t_1 evolution period. Because of the water-selective 180° pulse between the two gradients, the water magnetization is refocused by the second gradient. This 180° pulse results in a reversal of the sign of crosspeaks from water. The amplitude of fast exchanging resonances and resonances near the water frequency will be reduced depending on how much exchange occurs or how close the resonance is to the water frequency. The duration of the selective pulses is made sufficiently long to minimize the impact on resonances near the water chemical shift, but not so long as to allow too much exchange of fast exchanging resonances. For the vnd/NK-2 DNA complex at 35°C, a 45° pulse duration of 6–7 ms and a 180° pulse duration of 20–22 ms provided a good balance between the two effects. These selective pulses are sinc-shaped, and the corresponding effective field strength B1 is roughly 20 Hz. Crosspeaks within a few times this field strength from the water frequency, say up to 60 Hz (0.1 ppm from the water frequency on a 600 MHz ^{1}H frequency spectrometer), should experience some reduction in their amplitude due to the initial selective pulses and accompanying gradients.

Figure 3 shows that for both real and imaginary scans the water magnetization is brought to the $\pi/2$ (y) direction by the first high-power 90° pulse of the t_1 evolution period. Equal and

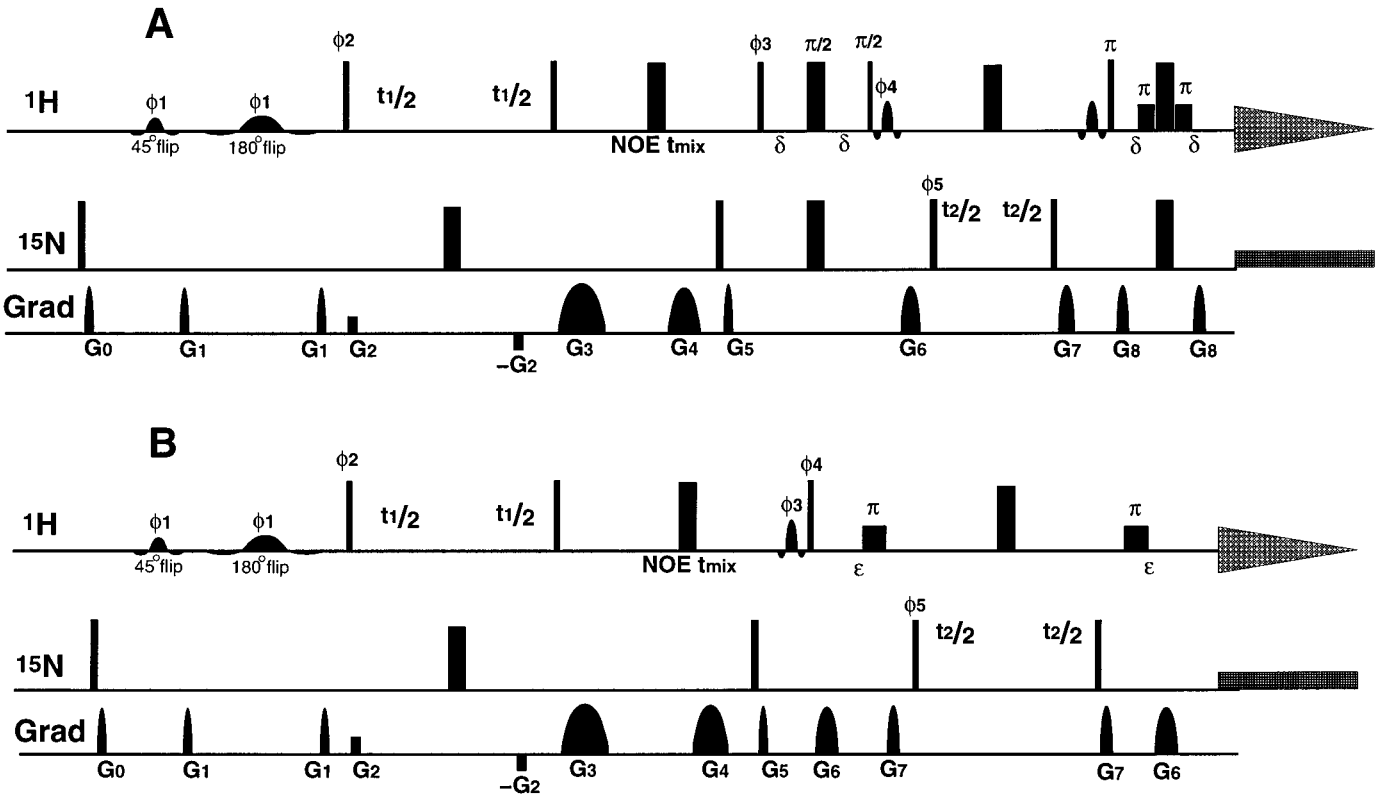

FIG. 2. Pulse sequences for the 3D ^{15}N-edited NOESY–HSQC and NOESY–HMQC with 45° water flipback. The tall, narrow rectangles correspond to high-power 90° ^{1}H and ^{15}N pulses, and the broader, tall rectangles correspond to high-power 180° ^{1}H and ^{15}N pulses. The short, broad rectangles correspond to low-power rectangular 90° pulses (~1 ms, 250 Hz). The taller ^{1}H shaped pulses, during the HSQC and before the HMQC portions of the pulse sequences, are sinc-shaped 90° pulses of ~2 ms duration. The two longer ^{1}H shaped pulses at the beginning of the sequences are a sinc-shaped 45° flip-angle pulse of ~6–7 ms duration and sinc-shaped 180° flip-angle pulse of ~20–22 ms duration. All pulses are applied at zero phase unless otherwise indicated. All ^{1}H pulses are applied at the carrier (H_2O) frequency. The rectangular gradient G2 has a strength of 2.5 G/cm along each axis and is in the $(+x, +y, +z)$ direction with a duration of 50 μs, followed by a delay of 50 μs. The initial t_1 time was set to a two-dwell delay in order to provide enough time for G2 and its delay. All other gradients are sine bell shaped with strengths of 25 G/cm along each axis. The phases for the NOESY–HSQC (A) are $\phi_1 = \pi/4, \pi/4, 5\pi/4, 5\pi/4$; $\phi_2 = 7\pi/4, 7\pi/4, 3\pi/4, 3\pi/4$; $\phi_3 = \pi, \pi, 0, 0$; $\phi_4 = 0$; $\phi_5 = 0, \pi$; acq. $= \pi, 0$. The States–TPPI protocol was used for phase-sensitive detection in the t_1 dimension by decrementing ϕ_1 and incrementing ϕ_2 by $\pi/2$ (also see Fig. 3). After each complex t_1 point, ϕ_4 is incremented by π. The TPPI protocol was used in the t_2 dimension by incrementing ϕ_5. The gradients G0, G1, and G2, and the directions and the delays that follow them, are the same as for the ROESY sequences of Fig. 1. The length of G3 is (tmix/2 − 0.5 ms), and G4 is (tmix/2 − 1 ms − G5), both followed by 0.5 ms delays. G3 and G4 are triple-axis along $(+x, +y, +z)$ and $(-x, +y, +z)$. The gradients G5, G6, G7, and G8 have durations of 0.22, 0.25, 0.2, and 0.4 ms, followed by 0.5 ms delays, and are triple-axis along $(+x, -y, +z)$, $(-x, -y, +z)$, $(-x, +y, +z)$ and $(+x, +y, +z)$. The delay $\delta = 2.2$ ms. For the NOESY–HMQC (B) the phases are $\phi_1 = \pi/4, \pi/4, 5\pi/4, 5\pi/4$; $\phi_2 = 7\pi/4, 7\pi/4, 3\pi/4, 3\pi/4$; $\phi_3 = \pi$, $\phi_4 = \pi, \pi, 0, 0$; $\phi_5 = 0, \pi$; acq. $= \pi, 0$. Phase-sensitive detection in t_1 and t_2 was done as in (A), with ϕ_3 being incremented by π each complex t_1 point. Gradients G0–G5 are the same as in (A). Gradients G6 and G7 have lengths of 3.0 and 0.2 ms, along $(+x, +y, +z)$ and $(+x, -y, +z)$, followed by 0.5 ms delays. The delay $\epsilon = 4.5$ ms.

opposite gradients dephase and refocus the water and other magnetization during the t_1 evolution period, which prevents radiation damping of the water magnetization (*17*). In the ROESY experiments, the water is then spin-locked in the $\pi/2$ direction, and in the NOESY experiments, the water is then rotated by the second high-power ^{1}H pulse to the $+z$ or $-z$ direction.

The ROESY–HMQC and NOESY–HMQC pulse sequences have only one additional pulse for water flipback, just prior to the first high-power ^{1}H 90 pulse of the HMQC portion of the sequences (*15*, *18*). This flipback pulse is a shaped, water-selective, 90° flip-angle pulse. For the NOESY–HMQC, the flipback pulse occurs at the end of the NOE mixing time. For the ROESY–HMQC, the ROE mixing time is followed by rotation of the spin-locked magnetization to the z axis. A short delay follows in which a gradient is applied, which serves the same purpose as a trim, or spin-lock purge, pulse, and then the water flipback pulse is applied. The first high-power ^{1}H pulse of the HMQC brings the water magnetization along $+z$. The following two low-power ^{1}H 90° pulses and the high-power ^{1}H 180° pulse cause a net zero rotation on the water magnetization, leaving it at $+z$ at the end of the pulse sequence. The G7 gradients in the NOESY–HMQC and G5 gradients in the ROESY–HMQC dephase and refocus the water magnetization, preventing radiation damping during the t_2 evolution period. A modified version of the WATERGATE water suppression

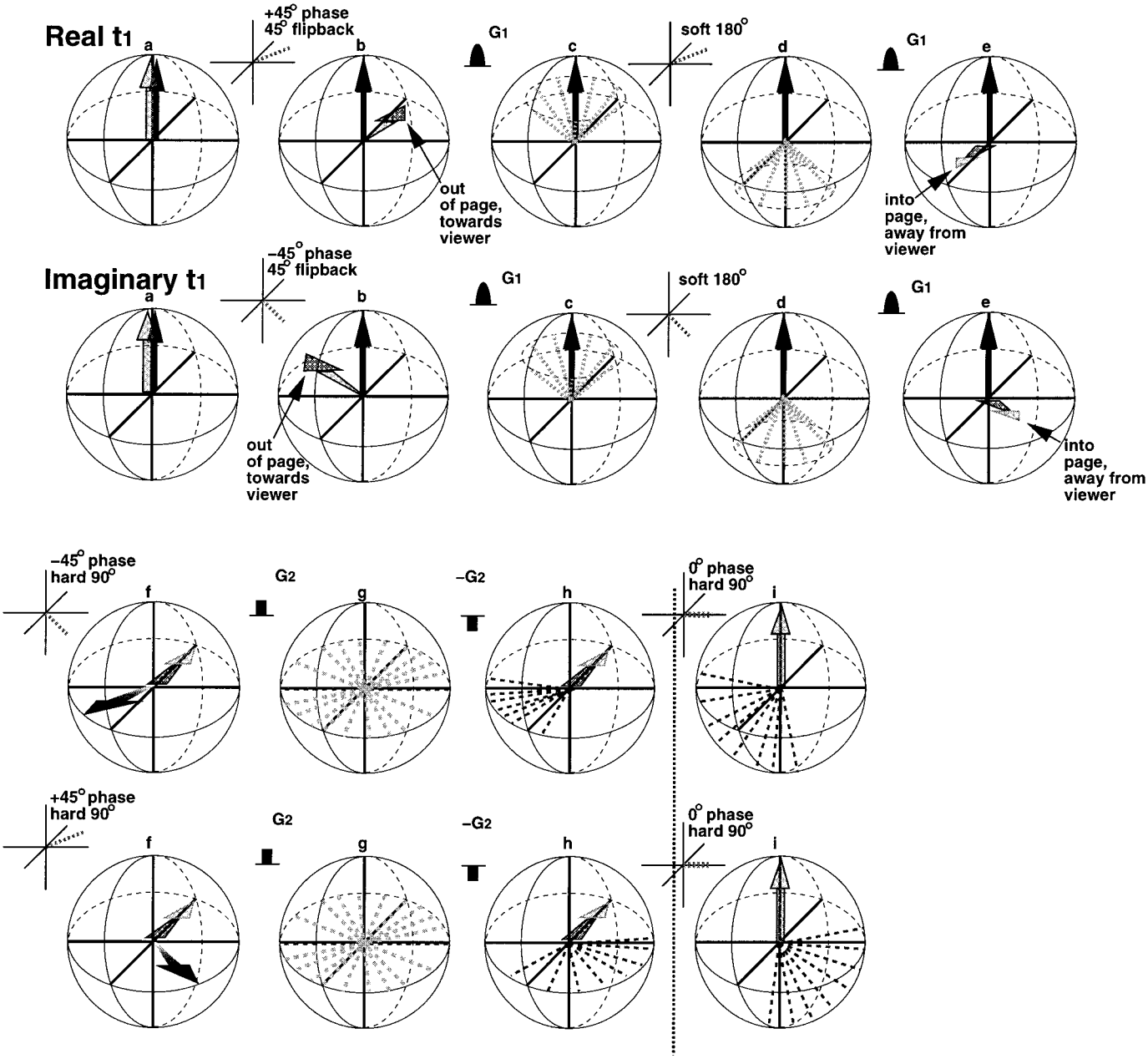

FIG. 3. The effects of the 45° water flipback and gradients on the water (lighter arrow) and nonwater (darker arrow) magnetization vectors are shown for the real and imaginary t_1 points. The first selective, shaped pulse is the 45° water flipback pulse, and it rotates the water magnetization 45° from the $+z$ direction. The phase of this pulse is indicated by the dotted line in the smaller axes appearing between points a and b. A gradient is then applied, G1, dephasing the water signal. A second selective, shaped pulse, at the same power and phase as the first, this time with a 180° flip-angle, rotates the dephased water signal 180°. The same gradient G1 is reapplied, refocusing the water magnetization 180° from its direction at point b, 135° from the $+z$ direction. A high-power 90° pulse then rotates both the water and the nonwater magnetization into the transverse, x–y plane, and the phase of this pulse is shown between points e and f. Notice that this high power pulse rotates the water magnetization to the $+y$ direction for both the real and the imaginary time points, while the nonwater signal differs by a phase of 90°, as required for phase sensitive detection in t_1. The gradient G2 defocuses the magnetization so that no radiation damping can occur during t_1, and the gradient $-$G2 refocuses the magnetization at the end of t_1. Since the carrier is set at the water frequency, no chemical shift evolution has occurred in the rotating frame for the water magnetization during t_1. In the ROESY experiment the spin-lock field is applied along the $+y$ direction at the end of the t_1 period, and so the full water magnetization is always spin-locked. In the NOESY experiment a high-power ^{1}H 90° pulse is applied along the x direction, and so the water magnetization is rotated to the z axis at the start of the NOE mixing time.

technique is employed during the HMQC to eliminate any residual transverse water signal (*15*). The ROESY–HSQC and NOESY–HSQC both use two flipback pulses during the HSQC and employ WATERGATE during the final reverse INEPT (*12, 13*).

All the pulse sequences in Figs. 1 and 2 use 45°-shifted

phase sensitive detection in the F1 dimension. This phase shift is needed so that crosspeaks from the water resonance have the same phase as the other crosspeaks in the spectrum. In 45°-shifted phase sensitive detection, the signal at the carrier, the signal from the water resonance, is always present with the same magnitude along the spin-lock axis during the ROE mixing time or the $+/-$ z direction during the NOE mixing time. Because of the 45° flip-angle water flipback, the full water magnetization, rather than just the 45° projection of the water signal, is spin-locked or brought to the $+/-$ z direction during the mixing time. Thus, flipback causes the crosspeaks from the water magnetization to be enhanced by a factor of the square root of two.

For the ROESY and NOESY experiments shown in Figs. 1B, 2A, and 2B, the phase cycling of the first high-power 90° pulse at the beginning of the t_1 period and the high-power 90° pulse at the end of the mixing time is used to cancel the major sources of axial signal that develop during the t_1 period and mixing time. To further ensure that residual axial signal does not interfere with ROE or NOE signal coming from the water magnetization, all the experiments are collected with the States–TPPI protocol in the t_1 dimension. With the States–TPPI protocol axial signal appears at the edge of the spectrum rather than at zero frequency (*19*). The NOESY sequences include a ^{1}H high-power 180° pulse halfway through the mixing time so that axial signal due to spin-lattice relaxation during the mixing time is cancelled for every scan. Gradients are applied during nearly all of the NOE mixing time in order to prevent water signal along $-z$ from relaxing due to radiation damping and to prevent artifacts that can arise in the water resonance plane due to the radiation damping feedback field (*20*). The inversion of the water signal during half the mixing time distinguishes the NOESY sequences here from earlier 4D, 3D, and 2D (homonuclear) NOESY pulse sequences with water flipback (*14, 15, 21, 22*). These earlier NOESY sequences require that the water signal be along $+z$ by the end of the mixing time. Except for experiments with very long mixing times, this requirement prevented the use of States–TPPI in these earlier sequences. The pulse sequence shown in Fig. 1A, the ROESY–HSQC experiment, uses a different phase cycle to cancel axial noise in the t_1 dimension than the other pulse sequences use. In this pulse sequence the first high-power 90° pulse and the acquisition phase, rather than the first high-power 90 pulse and the high-power 90 pulse following the mixing time, are used to cancel the axial noise. The reasons for this are purely historical, and the other pulse sequences could also be written using the acquisition phase cycle to cancel axial t_1 signal. Phase cycling the acquisition phase has the added advantage that any t_1 axial noise that somehow develops after the mixing time will also be canceled.

In order to minimize interactions with the ^{15}N magnetization that might appear at zero frequency and thus interfere with the ROE or NOE signal from water, two ^{15}N purges, ^{15}N 90° pulses followed by gradients, are employed. The first ^{15}N purge is at the beginning of the pulse sequence, to remove ^{15}N equilibrium magnetization, and the second one occurs at the end of the mixing time.

In the ROESY–HMQC, during the z filter following the ROE mixing time, NOE crossrelaxation can occur, so it is important to keep the z filter as short as possible. In both the ROESY–HMQC and NOESY–HMQC, the water flipback pulses during the mixing times make the conversion of the water crosspeak intensity into crossrelaxation rates problematic. In contrast, the ROESY and NOESY HSQC sequences have no water flipback pulses or other pulses during the mixing times that would interfere with the build-up of ROE or NOE crosspeaks from water to the amide protons.

Figure 4 compares the results of the ROESY–HMQC experiment with and without water presaturation during the recovery time. Except for the use of the presaturation field during the recovery time (1.4 s), the spectra were acquired and processed identically and are plotted at a threshold five times the rms noise level of each spectrum. The diagonal peaks for four backbone amide resonances of the vnd/NK-2 homeodomain and the ROE crosspeaks to these resonances are shown. The amides shown are slow-exchanging ($k_{ex} < 0.01$ s^{-1}) except for Phe8, which has a moderate rate (1 s$^{-1} > k_{ex} > 0.01$ s^{-1}) (*16*). Substantial improvement of the crosspeak intensity is seen when water flipback is employed. While the average improvement in the signal-to-noise ratio was 10% for the spectrum overall, for some signals the improvement was much more dramatic. For instance, in the spectrum with water presaturation, the crosspeaks for Tyr54 are too weak to be seen for the threshold shown in Fig. 4, but without presaturation, crosspeaks from the alpha and beta resonances are clearly evident. Water presaturation reduces the intensities of resonances that interact strongly with water. Most of the crosspeaks in Fig. 4 are from nonlabile protons, with the exception of the Ile47 to Trp48 HN–HN crosspeak, indicating that direct and relayed dipolar interactions with water are responsible for the reduction of the nonlabile resonance intensities.

Figure 5 compares the water resonance planes from the NOESY–HMQC and NOESY–HSQC experiments and compares the NOE crosspeaks for three arginine H$^{\epsilon}$ resonances. The majority of the signals correspond to resonances of fast-exchanging protons. These include the backbone amide protons of the unstructured N and C termini of the protein, which give the most intense (highest) crosspeaks, and the arginine guanidinium protons, which give the largest volume crosspeaks. Fast-exchanging amide protons at the beginnings of each of the three helices of the homeodomain, Lys10, Ala28, and Thr43, show large crosspeaks. For two residues, Leu26 and Ser27, the signal seen is likely dominated by their H$^{\alpha}$ resonances, which are degenerate with the water frequency. Several slow-exchanging amides also show crosspeaks at the water frequency, such as Thr13, Ser36, and Thr56, whose signals come in large part through relayed magnetization from their exposed hydroxyl groups. However, Thr9 and Thr41 have

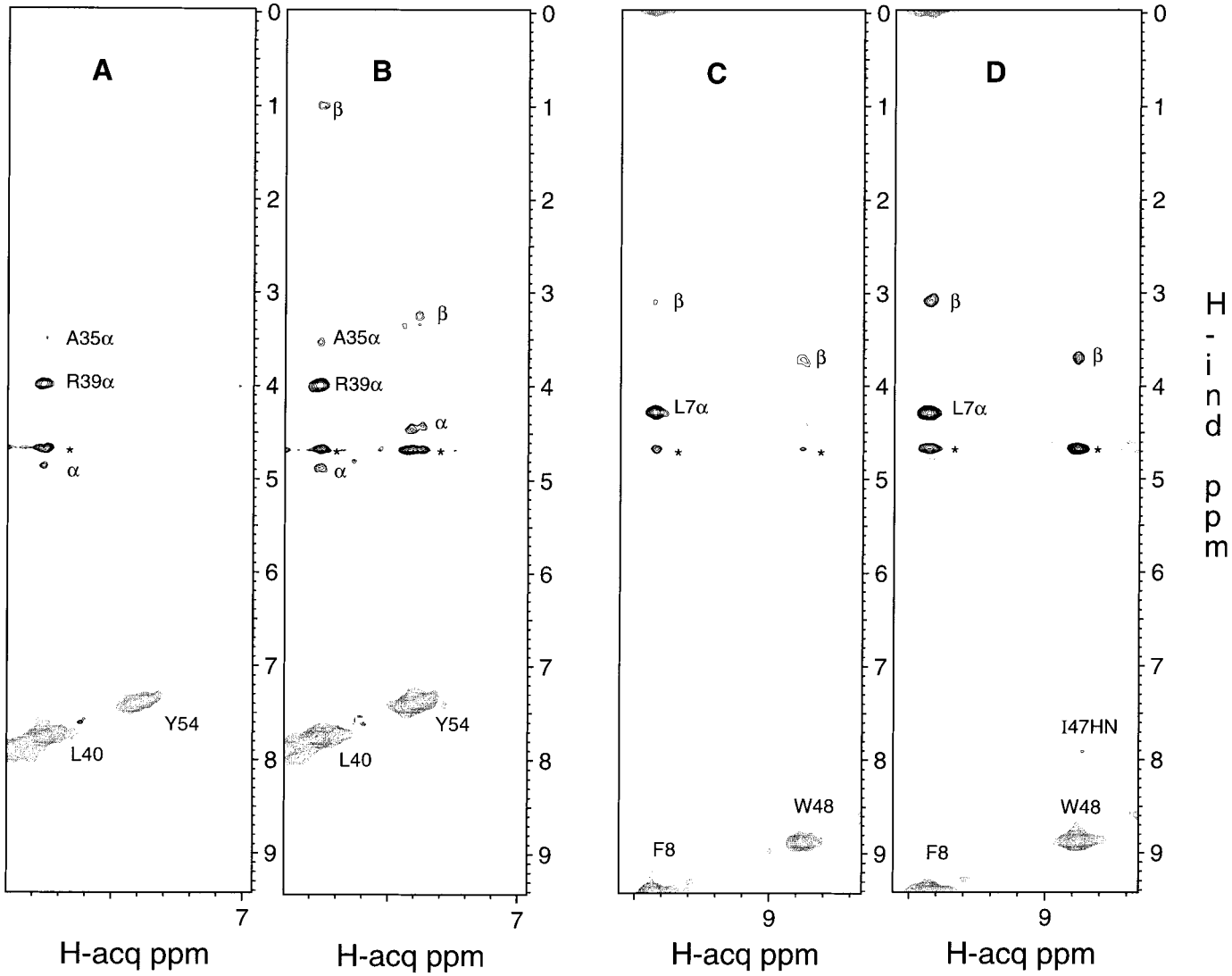

FIG. 4. Comparison of 45° water flipback ROESY–HMQC spectra of the vnd/NK-2 homeodomain DNA complex with (A and C) and without (B and D) water presaturation during the recovery delay (1.4 s). The backbone amide resonances are indicated by the labeled diagonal peaks. The crosspeaks labeled with a Greek letter alone are intraresidual ROE crosspeaks. The crosspeaks labeled with asterisks are from water. Because the presaturation field strength was very weak (B_1 = 13 Hz), a small, but sufficient amount of water signal remained to give crosspeaks to some of the amides in the presaturation experiment. The diagonal crosspeaks are positive, indicated by lighter shading, and all other labeled crosspeaks shown are negative. The spectra were recorded as 64* × 32 × 512* matrices, sixteen scans per point, with t_1 = 11.2 ms (F_1 = 5700.0 Hz), t_2 = 8.8 ms (F_2 = 1824.6 Hz), and t_3 = 61.4 ms (F_3 = 8333.3 Hz). Both spectra were linear predicted to double the size of t_1 and t_2, apodized with a shifted squared sine bell window function, and zero-filled in all dimensions. The ROE mixing time was 16 ms for both spectra.

neither fast-exchanging backbone amide protons nor exposed hydroxyl groups (*23*), and no crosspeaks are observed from water to their backbone amide protons. All together, about 30 backbone amides have little or no detectable crosspeaks from water, including some that are partially exposed to the solvent. Most interestingly, some slow-exchanging backbone amide

FIG. 5. Comparison of water resonance planes (4.644 ppm in the F1 dimension) and crosspeaks to three arginine H^{ϵ} resonances from NOESY–HSQC (top) and NOESY–HMQC (bottom) spectra of the vnd/NK-2 homeodomain DNA complex. Both spectra were recorded as 64* × 128 × 512* matrices, with t_1 = 11.2 ms (F_1 = 5700.0 Hz), t_2 = 42.0 ms (F_2 = 1520.5 Hz), and t_3 = 61.4ms (F_3 = 8333.3 Hz). Both spectra were linear predicted to double the size of t_1 and t_2, apodized with a shifted squared sine bell window function, and zero-filled in all dimensions. The NOE mixing time was 32 ms for both spectra. The region enclosed with dashed lines contains the crosspeaks from water to arginine guanidinium resonances. The horizontal line in this region corresponds to the three arginine H^{ϵ} resonances shown to the right. See text for additional details.

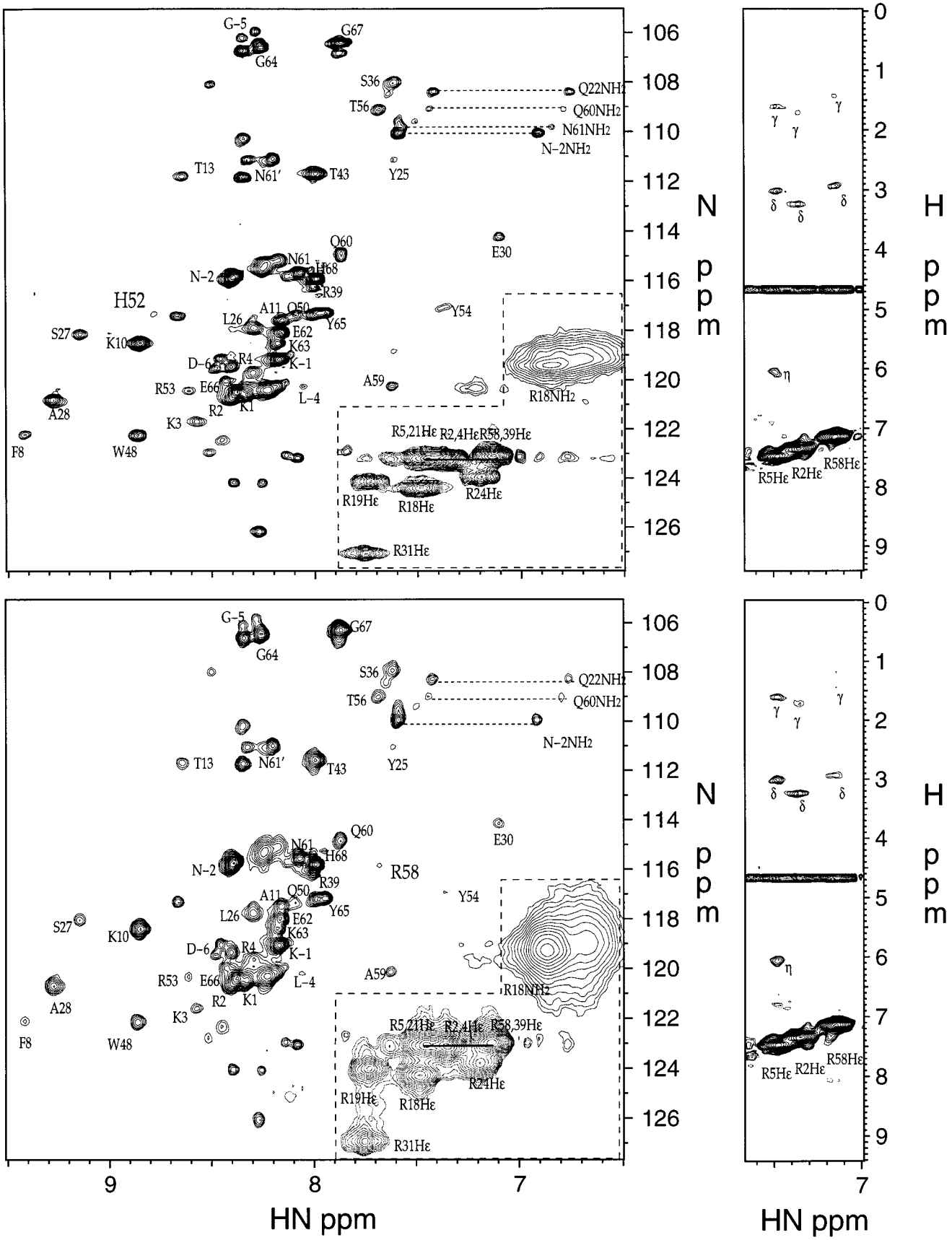
G-5
G67
G64
S36
Q22NH2
T56
Q60NH2
N61NH2
N-2NH2
T13
N61′
T43
Y25
Q60
E30
N61
H68
N-2
R39
H52
A11
Q50
Y54
L26
Y65
S27
K10
E62
K63
D-6
R4
K-1
A59
R18NH2
R53
E66
L-4
K1
A28
R2
K3
R5,21Hε
R2,4Hε
R58,39Hε
F8
W48
R19Hε
R18Hε
R24Hε
R31Hε
N ppm
H ppm
R58
R5Hε
R2Hε
R58Hε
HN ppm
HN ppm

protons have sizable crosspeaks from water and do not appear to be close to other fast-exchanging protein protons, including Phe8, Trp48, and Gln50, which might indicate the presence of long-lived waters near these residues (*9*).

Although ^{1}H–^{1}H scalar couplings cause broader ^{15}N linewidths in the NOESY–HMQC spectrum, some peak intensities (peak heights) are actually stronger (higher) in the NOESY–HMQC spectrum than in the NOESY–HSQC spectrum. The two spectra were acquired under comparable conditions, processed identically, and plotted in both cases at a threshold ten times the rms noise level for the water resonance planes and four times the noise level for the arginine crosspeaks. Water crosspeaks to the arginine side chain amide resonances, within the dashed box region in the lower right of the spectra, have approximately 30% more peak intensity (height) in the HMQC experiment. The remaining resonances, i.e., backbone amides and Gln/Asn side chain amides, are on average 30% more intense in the HSQC experiment. However, variations in the remaining peak intensities are not systematic. Two extreme examples are indicated in Fig. 5 by larger lettering, i.e., His52 and Arg58 backbone amides. The crosspeak from water to His52 is twice as strong in the HSQC spectrum, whereas the crosspeak to Arg58 is 37% stronger in the HMQC spectrum. These intensity differences arise due to relaxation processes occurring after the end of the mixing time, since the experiments are identical until this point. Because of this, the HSQC/HMQC intensity ratio measured for the water crosspeak to a particular amide should be the same for all crosspeaks to that amide. For the NOE crosspeaks to Arg2, Arg5, and Arg58 H^{ϵ} resonances, also compared in Fig. 5, the crosspeaks are on average 30% stronger in the HMQC spectrum, the same percentage that was observed comparing the water crosspeaks. Although, for reasons that are not entirely clear, the NOE crosspeaks to Arg58 H^{ϵ} are stronger in the HSQC spectrum. Much of the higher intensities seen in the HMQC experiment are due to the two extra delays in the HSQC experiment compared to the HMQC experiment. These delays occur just before and just after the ^{15}N evolution period, when all the ^{1}H and ^{15}N signal is along the z direction. For protons with very fast solvent exchange rates ($k_{ex} > 10\ s^{-1}$), such as arginine guanidinium protons, these extra delays result in significant loss of signal. Differences in the dipolar terms giving rise to single and multiple quantum relaxation could also account for some of the intensity variations.

Both the ROESY–HSQC and the NOESY–HSQC experiments were designed for our ongoing work in measuring protein–water cross-relaxation rates at protein–DNA interfaces. The major sources of t_1 axial signal are suppressed by the phase cycling of the 90° pulses at the beginning of the t_1 period and the end of the mixing time, and additionally for the NOESY experiment, the 180° pulse during the mixing time. The remaining residual axial signal should appear at the edge of the spectrum in the F1 dimension since the States–TPPI protocol is used. A ROESY–HSQC spectrum with a 1 ms mixing time and NOESY–HSQC spectrum with a 2 ms mixing time were recorded (both with data matrix sizes of 48* × 96 × 512*). No crosspeaks at the carrier (water) frequency were detectable in these two spectra except for a trace of signal for the fastest exchanging amide and guanidinium protons, which have the strongest water crosspeaks in the spectrum. The ROESY spectrum was recorded with a 1 ms mixing time instead of zero mixing time to accommodate the spinlock purge pulses. The NOESY spectrum was collected with a 2 ms mixing time to accommodate the gradients, gradient recovery delays, and high-power ^{1}H 180° pulse during the mixing time. In contrast with the HMQC experiments, no water flipback pulses are implemented during the ROESY–HSQC and NOESY–HSQC mixing times, as such would complicate the computation of the water crossrelaxation rates. The square root of two enhancement of the water crosspeaks aids the measurement of the rates by allowing the spectra to be recorded with fewer scans and shorter mixing times, reducing spin diffusion effects.

The use of water flipback significantly enhances signal in 3D ^{15}N-edited ROESY. This enhancement was observed for the signals from both labile and nonlabile protons. In addition, it should be straightforward to employ the Cavanagh–Rance–Kay sensitivity enhancement method at the end of the ROESY–HSQC and NOESY–HSQC pulse sequences to provide additional enhancement of the signal (*24*, *25*). Since there are fewer delays, the HMQC versions of the ROESY and NOESY can provide stronger signal for very fast exchanging protons. The HSQC versions are designed for the quantitative measurement of protein–water crossrelaxation rates, with no water-selective pulses during the mixing time, and with ^{15}N purges, phase-cycling, and a 180° pulse in the middle of the NOE mixing time to suppress artifacts in the water signal.

EXPERIMENTAL

All spectra reported here are from the complex of the vnd/NK-2 homeodomain bound to its cognate DNA at a 1.3 mM concentration at 308 K, 80 mM NaCl, and pH 6.0. The protein consists of a 77 amino acid peptide containing the 60 residue homeodomain plus 17 flanking residues, and the DNA is a duplex of 16 base pairs. Further sample preparation details have been described previously (*16*, *26*). The spectra were recorded on a Bruker AMX 600 MHz spectrometer. All spectra were processed with nmrPipe, and the spectra were plotted using nmrDraw (*27*).

REFERENCES

1. R. Ishima, P. T. Wingfield, S. J. Stahl, J. D. Kaufman, and D. A. Torchia, *J. Am. Chem. Soc.* **120,** 10534–10542 (1998).
2. D. C. Chatfield, A. Szabo, and B. R. Brooks, *J. Am. Chem. Soc.* **120,** 5301–5311 (1998).
3. S. Grzesiek, A. Bax, J. S. Hu, J. D. Kaufman, I. Palmer, S. J.

Stahl, N. Tjandra, and P. T. Wingfield, *Protein Sci.* **6,** 1248–1263 (1997).

4. I. Q. H. Phan, J. Boyd, and I. D. Campbell, *J. Biomol. NMR* **8,** 369–378 (1996).
5. J. W. Peng and G. Wagner, *Method Enzymol.* **239,** 563–596 (1994).
6. T. Szyperski, P. Luginbuhl, G. Otting, P. Guntert, and K. Wüthrich, *J. Biomol. NMR* **3,** 151–164 (1993).
7. Y. X. Wang, D. I. Freedberg, P. T. Wingfield, S. J. Stahl, J. D. Kaufman, Y. Kiso, T. N. Bhat, J. W. Ericson, and D. A. Torchia, *J. Am. Chem. Soc.* **118,** 12287–12290 (1996).
8. Y. Q. Qian, G. Otting, and K. Wüthrich, *J. Am. Chem. Soc.* **115,** 1189–1190 (1993).
9. G. Otting, E. Liepinsh, and K. Wüthrich, *Science* **254,** 974–980 (1991).
10. G. M. Clore, A. Bax, P. T. Wingfield, and A. M. Gronenborn, *Biochemistry* **29,** 5671–5676 (1990).
11. G. M. Clore, A. Bax, and A. M. Gronenborn, *J. Biomol. NMR* **1,** 13–22 (1991).
12. S. Grzesiek and A. Bax, *J. Am. Chem. Soc.* **115,** 12593–12594 (1993).
13. M. Piotto, V. Saudek, and V. Sklenar, *J. Biomol. NMR* **2,** 661–665 (1992).
14. D. B. Fulton and F. Ni, *J. Magn. Reson.* **129,** 93–97 (1997).
15. J. M. Gruschus and J. A. Ferretti, *J. Magn. Reson.* **135,** 87–92 (1998).
16. D. H. H. Tsao, J. M. Gruschus, L.-H. Wang, M. Nirenberg, and J. A. Ferretti, *Biochemistry* **33,** 15053–15060 (1994).
17. V. Sklenar, *J. Magn. Reson. Ser. A* **114,** 132–135 (1995).
18. P. Andersson, B. Gsell, B. Wipf, H. Senn, and G. Otting, *J. Biomol NMR* **11,** 279–288 (1998).
19. D. Marion, M. Ikura, R. Tschudin, and A. Bax, *J. Magn. Reson.* **85,** 393–399 (1989).
20. A. G. Sobol, G. Wider, H. Iwai, and K. Wüthrich, *J. Magn. Reson.* **130,** 262–271 (1998).
21. S. Grzesiek, P. Wingfield, S. Stahl, J. D. Kaufman, and A. Bax, *J. Am. Chem. Soc.* **117,** 9594–9595 (1995).
22. G. Lippens, C. Dhalluin, and J.-M. Wieruszeski, *J. Biomol. NMR* **5,** 327–331 (1995).
23. J. M. Gruschus, D. H. H. Tsao, L.-H. Wang, M. Nirenberg, and J. A. Ferretti, *J. Mol. Biol.* **289,** 529–545 (1999).
24. A. G. Palmer III, J. Cavanagh, P. E. Wright, and M. Rance, *J. Magn. Reson.* **93,** 151–170 (1991).
25. L. E. Kay, P. Keifer, and T. Saarinen, *J. Am. Chem. Soc.* **114,** 10663–10665 (1992).
26. J. Gruschus, D. H. H. Tsao, L.-H. Wang, M. Nirenberg, and J. A. Ferretti, *Biochemistry* **36,** 5372–5380 (1997).
27. F. Delaglio, S. Grzesiek, G. W. Vuister, G. Zhu, J. Pfeifer, and A. Bax, *J. Biomol. NMR* **6,** 277–293 (1995).